

# **Mechanics, Hydraulic and Coupled Hydromechanics of Fractured Rock Mass Investigated by Numerical Experiment**

Ki-Bok Min

*Department of Energy Resources Engineering, Seoul National University, Korea*

**ABSTRACT:** The DFN-DEM (Discrete Fracture Network-Discrete Element Method) approach uses DFN as the geometry of fractured rock and DEM for the solution technique to simulate the hydraulic and mechanical behaviour of fractured rock. This overview paper intends to summarize the applications on fractured rock using the DFN-DEM approach with the focus upon the determination of mechanical and hydraulic properties of fractured rock and their stress dependencies. The establishment of methodologies and actual applications in a site considered for geological repository of nuclear waste are introduced.

## **1 Introduction**

An engineering application in and on rock masses must consider the presence of fractures for design, construction and operation, because the existence of fractures influences the hydraulic and mechanical properties of rock masses. Mechanical properties of fractured rock masses are substantially different from those of intact rock. Fractures also act as main pathways of fluid flow, especially in hard crystalline rocks. Apertures of fractures can change due to normal stress-induced closures or openings and to shear stress-induced dilations. Hence, the permeability of fractured rock masses is stress-dependent (Rutqvist and Stephansson, 2003). To obtain the hydro-mechanical properties of fractured rock, one can conduct in situ experiments in a relevant scale, which can vary from a decimeter to tens of meters. However, field testing in large scale is a very difficult task in terms of cost and control of boundary conditions, among others. If this is the case, a 'numerical' experiment can be an alternative provided that the experiment can consider the various fracture geometry and its constitutive relations used for each numerical experiment.

The objective of the paper is to introduce a series of numerical experiments that have been used to obtain mechanical and hydraulic properties of fractured rock and their stress dependencies. The paper concludes with a brief introduction of the actual application to a site considered for a geological repository of nuclear waste.

## 2 Methodology and geological data

The DFN-DEM (discrete fracture network-discrete element method) approach (Min and Jing, 2004) uses fracture system realizations as the geometric models of the fractured rock masses and conducts numerical experiments using a DEM program, UDEC (Itasca, 2000), for the calculation of mechanical and hydraulic properties. In this study, ten series of DFN models were generated to ensure that the calculated results were not dependent upon one specific realization and to produce more representative behaviour of the fractured rock masses. Additional numerical experiments investigating the effect of stresses were conducted on determined REV (Representative Elementary Volume), which led to empirical equations that account for the effect of stress on mechanical and hydraulic properties. If needed, the mechanical and hydraulic properties corresponding to different stress levels can be passed on to a large-scale model for the equivalent continuum analysis (Min et al., 2004c). Figure 1 shows the boundary conditions for the determination of mechanical properties and stress dependent permeability used in the UDEC simulations. The geological data were extracted from an extensive site investigation programme at Sellafield, UK, conducted by Nirex UK Ltd (Table 1).

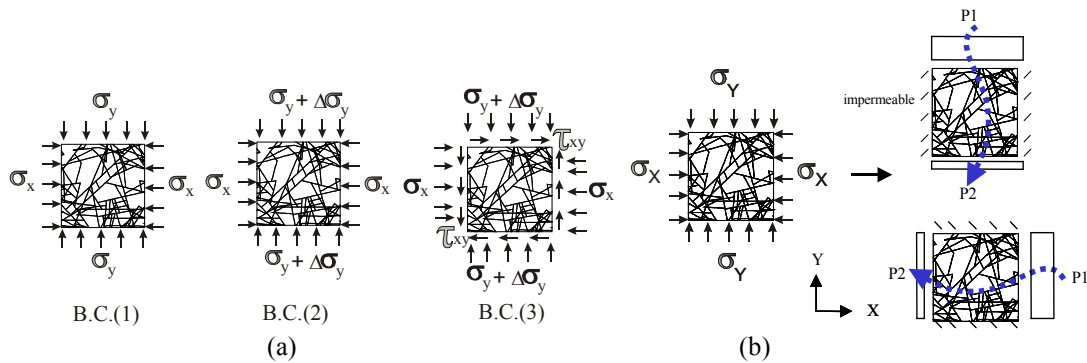


Figure 1. Boundary conditions for the determination of (a) mechanical properties and (b) stress-dependent permeability of fractured rock masses (Min and Jing, 2003; Min et al., 2004b).

Table 1. Model parameters used for the study (Min and Jing, 2003, 2004, Min et al., 2004a,b).

Intact rock	Elastic modulus (GPa)/Poisson's ratio	84.6/0.24
Fractures	Dip/dip direction (4 sets)	8/145, 88/148, 76/21, 69/87
	Fisher constants (4 sets)	5.9, 9.0, 10.0, 10.0
	Fracture density per set (m <sup>-2</sup> )	4.6
	Normal/Shear stiffness (GPa/m)	434/434
	Friction angle (°)/Dilation angle (°)	24.9/5
	Critical shear displacement for dilation, U <sub>cs</sub> (mm)	3
	Joint Roughness Coefficient (JRC, scale 0.3 m)	3.85
	Joint wall compressive strength (MPa)	112.21
	Initial mechanical/hydraulic aperture at 1 <sup>st</sup> cycle (μm)	77/65
Maximum/Initial/Residual aperture at 4 <sup>th</sup> cycle (μm)	50/30/5	

### 3 Mechanical properties of fractured rock masses

Equivalent mechanical properties were calculated by the numerical experiments based on the DFN models with varying side lengths from 0.25 m to 8 m. Figure 2 presents the normalized elastic moduli in the  $x$ -directions ( $E_x$ ) obtained from ten DFN realizations and predicted and calculated  $E_x$  in rotated axes. At the side length less or equal to 1 m, the ranges of  $E_x$  changes are notably larger (Figure 2a). However, the scattering of the results clearly narrows down with increase of the side lengths of the DFN models and points to the possible existence of an REV. The mean value of the normalized elastic moduli in the  $x$ -direction is reduced to about 43%. The DFN models are rotated in six clockwise directions with a  $30^\circ$  interval ( $0^\circ$ ,  $30^\circ$ ,  $60^\circ$ ,  $90^\circ$ ,  $120^\circ$  and  $150^\circ$ , respectively) with the same boundary conditions to examine whether the calculated elastic properties could be represented by an elastic compliance tensor (Figure 2b). The calculated properties were compared with the predicted ones using fourth order tensor transformation. The results show that the numerical results from the small scale models do not match well with the predicted values (Min and Jing, 2003). However, as the size of model increases, the numerical results match increasingly well with the predicted values (Figure 2b), indicating that the property at larger sizes ( $>5$  m side length) can be approximated by a fourth-order tensor.

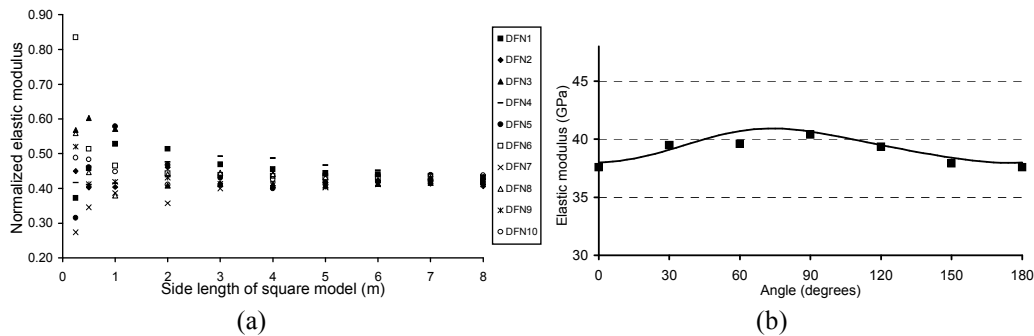


Figure 2. (a) Calculated elastic moduli in  $x$  direction ( $E_x$ ), (b) comparison between predicted (line) and calculated (square)  $E_x$  in rotated axes with the side length 5 m (Min and Jing, 2003).

### 4 Permeability of fractured rock masses

Equivalent permeability tensor was calculated by the numerical experiments based upon the same DFN models with varying side lengths from 0.25 m to 10 m. The initial hydraulic aperture for this analysis was  $65 \mu\text{m}$  in all fractures (Table 1). Figure 3 shows the results of calculated

values of permeability in x-direction ( $k_{xx}$ ) and the comparison of predicted and calculated permeability. The variances of calculated permeability components become smaller as the model size increases, and the permeability values maintain constant ranges after a certain size indicating the existence of an REV (Figure 3a).

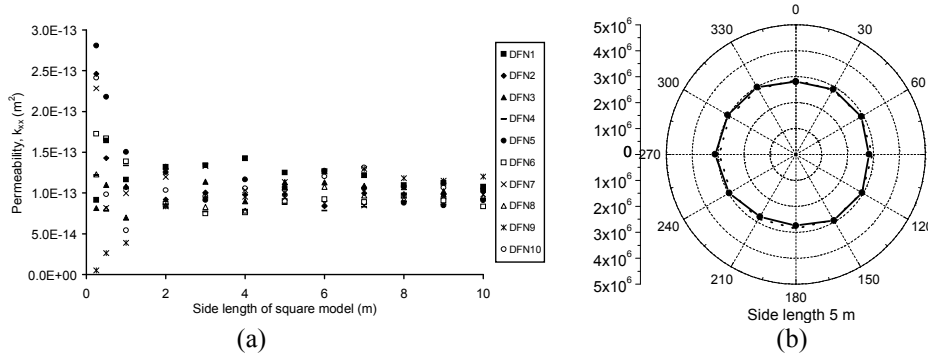


Figure 3. (a) Calculated permeability in x-direction ( $k_{xx}$ ), (b) comparison of predicted and calculated permeability expressed in the reciprocal of square roots (Min et al., 2004a).

The numerical experiments were conducted for the rotated DFN models to calculate directional permeability to check whether the calculated directional permeability in the pertinent regions can be represented approximately as a tensor. The directional permeability from a permeability tensor will appear as a perfect ellipse on a polar diagram when it is expressed in the reciprocal of square root (Long et al., 1982). The results show that the directional permeability does not conform to an ellipse for models of side length  $< 5$  m (Min et al., 2004a). As the side length of the model increases, the tendency to approach an ellipse by the numerical data becomes stronger (Figure 3b).

In this study, the following unified two criteria for the appropriateness of an equivalent continuum approach are suggested: ‘Coefficient of variation’ to evaluate the variation from the multiple realization of stochastic DFN and ‘mean prediction error’ for the evaluation of error involved in the prediction of tensor in rotated axes. From these criteria, the size of  $5 \text{ m} \times 5 \text{ m}$  was established as adequate representative REV for both mechanical (presented in the previous section) and hydraulic properties and was used for the additional numerical experiments investigating the effect of stresses that will be introduced in the subsequent sections.

## 5 Stress dependent mechanical properties of fractured rock masses

To consider the stress dependency, numerical experiments are repeated at different stress levels. The Barton-Bandis (BB) model is used as the constitutive model of the fractures (Barton, 1982)

to consider the effect of stress. Figure 4 presents the elastic moduli in the  $x$ -direction and Poisson's ratios, with the increase of the boundary stress. Significant increases of elastic moduli were observed with the stress increase. A simple empirical equation is proposed to relate the rock mass elastic modulus ( $E_m$ ) to the magnitude of stresses ( $\sigma$ ), elastic modulus of the intact rock ( $E_i$ ) and a sensitive parameter ( $S_m$ ) (Min and Jing, 2004). The Poisson's ratios decrease from over 0.8 at 1 MPa to 0.65 at 40 MPa (Figure 4(b)). However, its stress dependency is not as strong as in the case for elastic modulus. What is startling is that all of Poisson's ratio values are higher than the limit of Poisson's ratio for the isotropic case, 0.5, regardless of the magnitude of stress. High fracture densities and connectivities of the geometry used for this study and the two dimensional approximation are reasons for this high Poisson's ratio (Min and Jing, 2004).

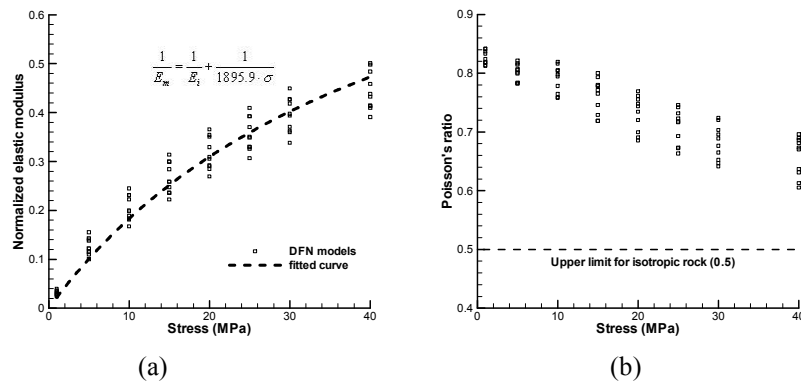


Figure 4. (a) Elastic moduli and (b) Poisson's ratio versus stress (Min and Jing, 2004).

## 6 Stress dependent permeability of fractured rock masses

A series of numerical experiments were conducted using various stress conditions for calculating the corresponding flow fields and changes in the permeability of the region. Numerical experiments were conducted in two ways: (1) increasing the overall stresses with a fixed ratio (stress ratio,  $k$ ) of horizontal to vertical stress; and (2) increasing the differential stresses (i.e., the difference between the horizontal and vertical stresses) while keeping the magnitude of vertical stress constant. A step-wise normal stiffness of fracture was implemented to represent the non-linear normal stress-normal closure deformation response, and special emphasis was given to the role of fracture shear dilation and associated channelling of flow for the investigation of stress-dependent permeability, adopting an elasto-perfectly-plastic shear behaviour of the fracture.

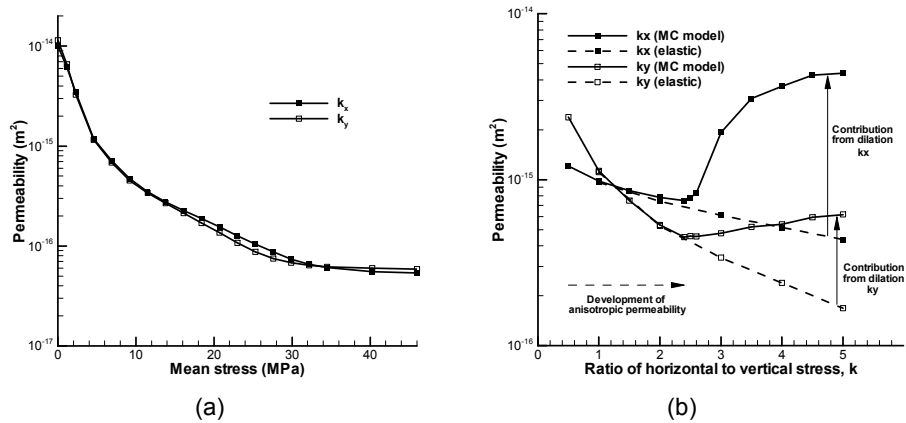


Figure 5. Permeability ( $k_x$  and  $k_y$ ) versus stress with (a) fixed ratio of horizontal to vertical stresses = 1.3, (b) change in stress ratio (Min et al., 2004b).

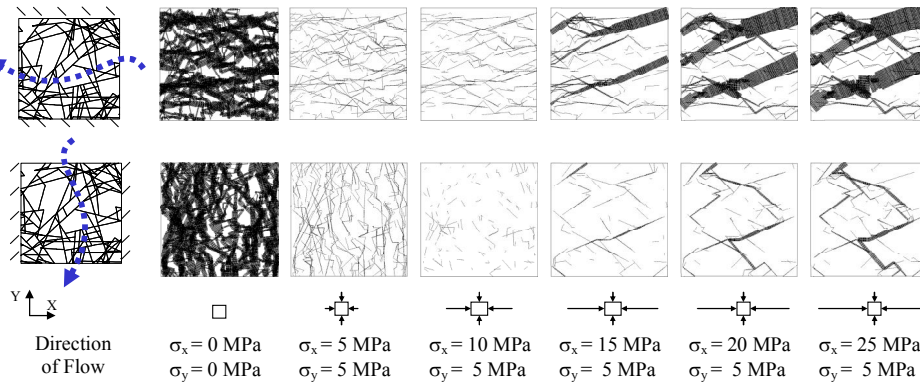


Figure 6. Enhanced fluid flow due to shear slip from increased horizontal rock stress. Shear dilation causes the increase of permeability by a factor of six when the range of allowable change of aperture is from 5 microns to 50 microns (Min et al., 2004b).

Figure 5 shows the permeability change with stress increases with fixed stress ratio and increasing  $k$  ratio. As shown in Figure 5(a), because of the dominating fracture closure with the increasing normal stresses, the permeability of the model decreases accordingly. The reduction of permeability is more than two orders of magnitude, and anisotropy in permeability is not significant, mainly because the stress ratio  $k$  is close to isotropic stress. The non-linear normal stiffness of fractures led to more sensitive responses of permeability change at lower stress. This implies permeability at shallow depth is more sensitive to stress changes than at greater depth, as reported in Rutqvist and Stephansson (2003). In Figure 5(b), the effect of shear deformation is more significant. Results are compared with the ones from a pure elastic fracture model that excludes failure and dilation. The pure elastic and the elastoplastic models show a similar response until the stress ratio  $k$  reaches approximately 2.5. At this point and afterwards, some fractures in the fractured rock masses start to fail in shear, and, with continued shear

dilation, notable differences between the models are observed. The increase of permeability stabilizes after a certain  $k$  ratio, because the shear dilation of a fracture does not continue after their critical shear displacement is reached.

A notable channelling flow effect caused by stress-induced fracture dilation is observed (Figure 6). As large shear dilations are concentrated in a smaller part of the fracture population with near-critical orientations, good connectivity, and long trace lengths, the rest of the fracture population, especially the sub-vertical ones, still undergo the normal closures without any shear dilation. This situation causes a high contrast in aperture values between the fractures. Therefore, a few fractures with increased apertures become the major pathways of fluid flow (Min et al, 2004b).

## **7 Application to the geological repository model in Forsmark**

The established DFN-DEM approach was applied to the geological repository in Forsmark, which is chosen as the sole candidate site for Swedish repository (Min and Stephansson, 2009). That study was composed of three steps as shown in Figure 7. In the first step, three-dimensional thermomechanical analysis was conducted to obtain the full stress history in the far-field around the repository. The analysis used COMSOL MULTIPHYSICS, which is a flexible partial differential equation solver that uses the finite element method (COMSOL, 2008). The sizes of the models were 2 km x 2 km x 0.8 km (depth) and 600 m x 600 m x 13 m (depth) for the regional and repository scales, respectively.

In the second stage, stress history obtained from the first stage was used to establish the boundary conditions to be used in the DFN-DEM approach. DFN was constructed at selected points in mid- and far-field based upon the site investigation data from Forsmark and Laxemar (SKB, 2006). The study was able to quantify the extent of shear dilation under the specific stress state and the nature of irreversibility of permeability could be studied through application of stress release expected to occur after cooling of the spent fuel.

Finally, the third stage was devoted to integration of outcomes from the first and second stages to quantify the shear slip potential and corresponding permeability changes.

To monitor the evolution of important variables, such as temperature and stress, monitoring points were established in four hypothetical boreholes as indicated in Figure 8.

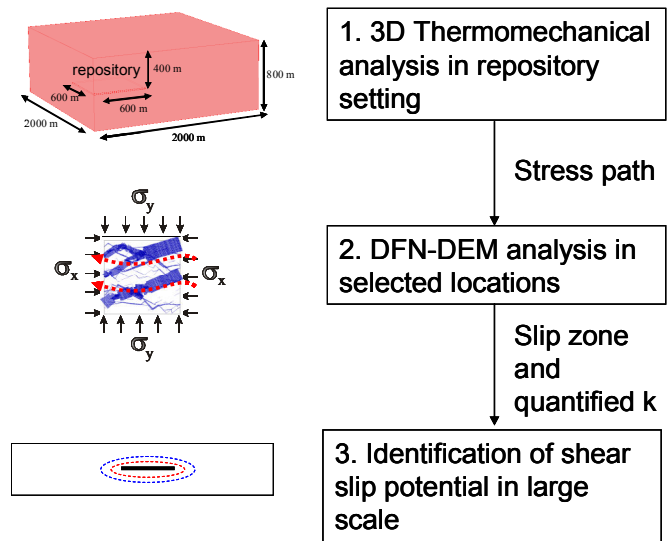


Figure 7. Three components of the modeling work (Min and Stephansson, 2009)

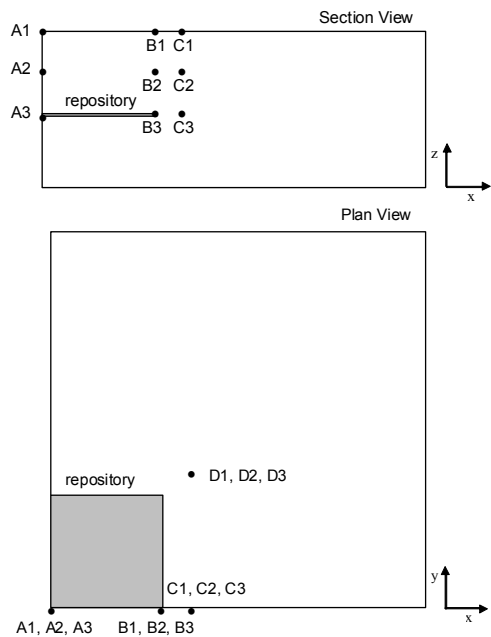


Figure 8. Locations of monitoring points around repository (Min and Stephansson, 2009)

Figure 9(a) shows the evolution of stresses in the horizontal direction (mainly compressive) at various points at the repository level after the emplacement of spent fuel. The maximum compressive stress of 20 MPa was observed at the center of the repository after approximately 100 years. At the periphery of the repository, the magnitudes were smaller, with a maximum compressive stress of about 10 MPa. Maximum horizontal compressive stress was observed in the center of the repository at repository level and horizontal stresses were isotropic. Also, notable anisotropic horizontal compressive stresses were observed near the periphery of the

repository. Figure 9(b) shows the transition of stress state plotted in terms of Mohr Circle at locations A3 and A1. The friction coefficients used for upper and lower bounds were 1.0 and 0.6, respectively. In location A3, which is at a depth of 400 m, the possibility of failure greatly increased after 100 years due to the comparatively high horizontal stress. After 1,000 years, the contribution of thermal stress to the failure of fracture was less significant due to the relatively homogeneous increase of thermal stress in both horizontal and vertical directions.

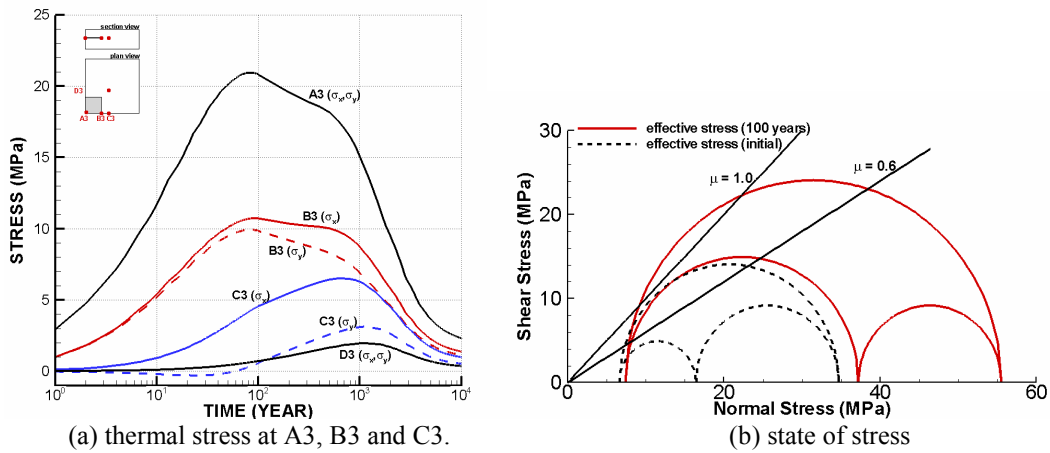


Figure 9. Evolution of thermal stresses at selected locations and state of stress 100 years after the emplacement of spent nuclear fuel (Min and Stephansson, 2009).

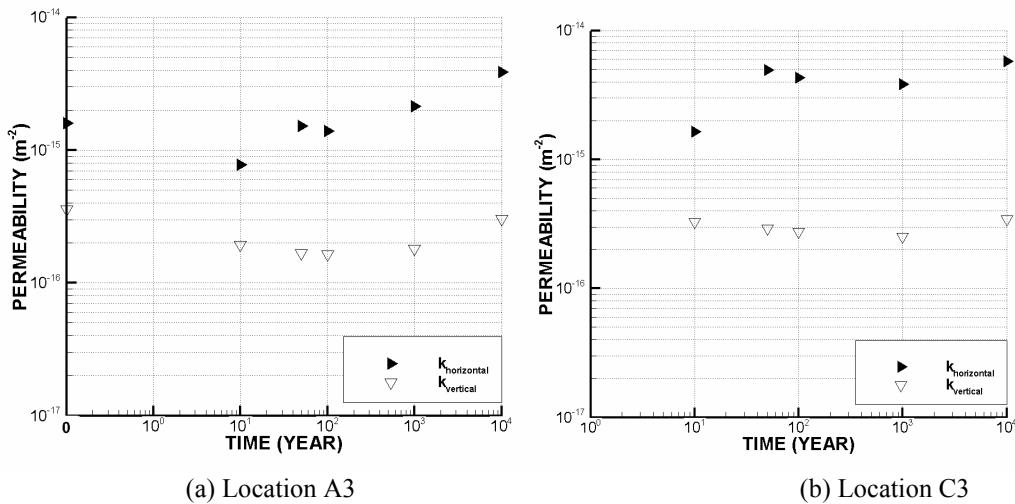


Figure 10. Permeability change versus time at monitoring points A3 and C3 (Min and Stephansson, 2009).

Permeability measurements were conducted on six models of DFN using two sets of stress paths at selected locations. The selected locations were A3 and C3 at the repository level for which a reasonable possibility of shear slip and permeability increase was expected. Final

stresses were calculated by superimposing the generated thermal stress on in-situ stress. Figure 10 shows the permeability change due to the stress changes from heating for six sets of DFNs. The major mechanism of permeability change in four out of six of the models (DFN3, DFN6, DFN7, DFN10) was normal deformation (closure) of fractures without shear slip. This can be explained by the lack of optimally oriented fractures with respect to the stress orientation and poor connectivity in these models. Only two models (DFN5 and DFN9) showed shear slip and permeability increases up to a factor of four.

An interesting observation is the non-reversibility of the permeability for the time scale of 10,000 years. Unlike the models for which normal closure dominated, permeability did not recover in the two models in which shear slip was a dominant mechanism. This demonstrates the importance of irreversibility of permeability once shear slip does occur. Vertical permeability at the repository level was insensitive to stress changes due to the fact that vertical fractures were largely closed at this magnitude of stress.

## **8 Conclusion**

The current paper presents the overview of the author's own work for the development of a numerical experiment to investigate the mechanical and hydraulic properties and their stress dependencies in fractured rock. The outcome of this paper has implications not only for geological repository but also for other energy and environmental engineering applications, including CO<sub>2</sub> underground storage and Enhanced Geothermal Systems (EGS) in which coupled hydromechanics is the main mechanism for the leakage of CO<sub>2</sub> and permeability enhancement of fractured geothermal reservoir. The main conclusions of this work can be summarized as follows.

- (1) The methodology for the determination of mechanical properties of fractured rock masses was developed using a DFN-DEM approach.
- (2) The results show that REV existed for the fractured rock masses with the given geological data and elastic compliance tensors, and permeability could be represented in tensor form.
- (3) Mechanical properties of fractured rock masses are highly stress-dependent.
- (4) Permeability can increase or decrease with stress increase depending upon the state of stress rather than a single component or an averaged value of stresses.
- (5) Stress-induced channelling effects of fluid flow were found from the numerical modelling.
- (6) The zones of fracture shear slip during the operation of the geological repository were

examined by combining thermomechanical analysis and the DFN-DEM approach. The study reveals that the fractures of different orientations are vulnerable to shear slip at various locations in and around a deep geological repository.

## 9 ACKNOWLEDGEMENT

Financial assistance for this overview paper was provided by the Korea Ocean Research and Development Institute (PMS198, 0456-20100022). European Commission (FIKW-CT-2000-00066), the Swedish Nuclear Power Inspectorate (SKI) and Swedish Radiation Safety Authority (SSM) were the main sponsors of the work included in the paper. Their sponsorship is gratefully acknowledged. Special thanks are extended to Dr Lanru Jing of the Royal Institute of Technology, Professor Ove Stephansson of GeoForschungsZentrum (GFZ), and Dr. Jonny Rutqvist and Dr. Chin-Fu Tsang of Lawrence Berkeley National Laboratory for their advice and collaborations.

## 10 References

- Itasca Consulting Group 2000, *UDEC User's Guide*, Ver. 3.1, Minnesota.
- Long J.C.S., Remer J.S., Wilson C.R., Witherspoon P.A. 1982, Porous media equivalents for networks of discontinuous fractures, *Water Resour Res*; 18(3): 645-658.
- Min K.-B., Jing L., 2003, Numerical determination of the equivalent elastic compliance tensor for fractured rock masses using the distinct element method, *Int J Rock Mech Min Sci*; 40(6): 795-816.
- Min K.-B., Jing L., 2004, Stress dependent mechanical properties and bounds of Poisson's ratio for fractured rock masses investigated by a DFN-DEM technique, *Int J Rock Mech Min Sci*; 41(3): 431-432.
- Min K.-B., Jing L., O Stephansson, 2004a, Determining the Equivalent Permeability Tensor for Fractured Rock Masses Using a Stochastic REV Approach: Method and Application to the Field Data from Sellafield, UK, *Hydrogeology Journal*; 12(5): 497-510.
- Min K.-B., Rutqvist J., Tsang C.-F., Jing L., 2004b, Stress-dependent permeability of fractured rock mass: a numerical study, *Int J Rock Mech Min Sci*; 41(7): 1191-1210.
- Min K.-B., Rutqvist J., Tsang C.-F., Jing L., 2004c, Thermally induced mechanical and permeability changes around a nuclear waste repository – a far-field study based on equivalent properties determined by a discrete approach, *Int J Rock Mech Min Sci* (accepted for publication).
- Min KB, Stephansson O, Potential for shear slip due to thermo-mechanical loading of a deep geological repository for nuclear waste, Hudson et al. (eds), In: *Int Symp Rock Mech "Rock Characterization, Modeling and Engineering Design Method,"* 2009, Paper No. 239.
- Rutqvist J., Stephansson O. 2003, The role of hydromechanical coupling in fractured rock

engineering, *Hydrogeology Journal*; 11:7-40.

Swedish Nuclear Fuel and Waste Managing Company, 2006. Long-term safety for KBS-3 repositories at Forsmark and Laxemar – a first evaluation, SKB TR-06-09.